PAPER

Photoinduced-reset and multilevel storage transistor memories based on antimony-doped tin oxide nanoparticles floating gate

IOP Publishing Nanotechnology
Nanotechnology 33 (2022) 025201 (9pp) https://doi.org/10.1088/1361-6528/ac2dc5

Photoinduced-reset and multilevel storage transistor memories based on antimony-doped tin oxide nanoparticles floating gate

Risheng Jin, Keli Shi*, Beibei Qiu and Shihua Huang*

College of Physics and Electronic Information Engineering, Zhejiang Normal University, Jinhua, Zhejiang 321004, People's Republic of China

E-mail: shikl@zjnu.edu.cn and huangshihua@zjnu.cn

Received 25 May 2021, revised 20 September 2021
Accepted for publication 6 October 2021
Published 22 October 2021

Abstract

Recently, antimony-doped tin oxide nanoparticles (ATO NPs) have been widely used in the fields of electronics, photonics, photovoltaics, sensing, and other fields because of their good conductivity, easy synthesis, excellent chemical stability, high mechanical strength, good dispersion and low cost. Herein, for the first time, a novel nonvolatile transistor memory device is fabricated using ATO NPs as charge trapping sites to enhance the memory performance. The resulting organic nano-floating gate memory (NFGM) device exhibits outstanding memory properties, including tremendous memory window (~85 V), superhigh memory on/off ratio (~10^9), long data retention (over 10 years) and eminent multilevel storage behavior, which are among the optimal performances in NFGM devices based on organic field effect transistors. Additionally, the device displays photoinduced-reset characteristic with low energy consumption erasing operation. This study provides novel avenues for the manufacture of simple and low-cost data storage devices with outstanding memory performance, multilevel storage behavior and suitability as platforms for integrated circuits.

Supplementary material for this article is available online

Keywords: antimony-doped tin oxide nanoparticles, floating gate, organic transistor memory, photoinduced-reset, multilevel storage

(Some figures may appear in colour only in the online journal)

1. Introduction

Organic field effect transistor (OFET) type nonvolatile memories have been seen as a promising candidate for next-generation electronic devices due to the advantages of non-destructive read-out, facile solution processability, low cost fabrication and flexibility [1–4]. Currently, based on charge-storing medium between the semiconductor layer and dielectric layer, OFET-type memories can be generally categorized into: [5, 6] (i) ferroelectric OFET memory, (ii) polymer electret OFET memory, and (iii) floating gate OFET memory. Among them, the floating gate memory is the most studied configurations, in which continuously conducting materials with a planar structure or discrete nanoparticles (NPs) are utilized as charge trapping sites for charging or releasing during the programming and erasing procedures [7–9]. However, the floating gate memory with the planar structure is considered to reach its limitations due to the fundamental scaling-down and current leakage problems [10]. Therefore, discrete NPs are employed as charge storage sites to fabricate nano-floating gate OFET memories (NFGO-FETMs) due to their suppression of charge leakage effect, capacity to be scaled down, multilevel storage, superior reliability and high speed of operation [11].

With the advent of the information age, the requirement of memory device is developing, such as increased density, faster storage speed, lower power consumption and more facile fabrication [12, 13]. Several possible solutions have

* Authors to whom any correspondence should be addressed.

Table 1. Comparison of current work with representative organic nano-floating gate memories.

Floating gate material	Memory window	Memory on/off ratio	Data retention time	Multilevel data storage	Light operation	References
$CoFe_2O_4$ nanoparticles	73.84 V	2.98×10^3	1000 s	N/A	N/A	[11]
PCBM	22.1 V	10^2	12 000 s	2 bits	Erase	[31]
C_{60}	~20 V	10^5-10^6	10 000 s	N/A	Erase	[34]
CdSe quantum dot	N/A	10^5	10 000 s	N/A	Erase	[35]
Conjugated polymer nanoparticles	35 V	10^4	10 000 s	N/A	N/A	[36]
$MAPbBr_3$	N/A	10^4	40 000 s	~2 bits	Program	[37]
ATO NPs	~85 V	10^9	10 000 s	2 bits	Erase	In this work

been proposed to boost the data storage capacity. One is the reduction of the memory cell size, but Moore's Law gradually approaches the physical limit and the precision of photolithography process is limited [14, 15]. Another effective method to expanse the storage capacity is to develop multilevel memory [16, 17]. For example, Yang *et al* demonstrated a multilevel photonic memory with a vertical OFET, in which 8 distinctive current levels were obtained and maintained over a long time period [15]. Tran *et al* reported multilevel nonvolatile OFET memory using a lithium-ion-encapsulated fullerene as a charge trapping layer [18]. Four logic states with high discrepancies were clearly observed. In addition to increasing the storage space, the multilevel memory effects can also be used to simulate the behavior of synapses, showing potential for the neuromorphic circuit applications [19, 20]. In order to achieve multilevel date storage, memory properties, such as memory window and retention time, need to be enhanced [16, 17]. To date, metallic NPs, particularly gold (Au) NPs, are widely used as floating gate materials in NFGOFETMs owing to their suitable work function and high air stability [21]. The floating gate layer based on metallic NPs is commonly deposited by the expensive high-vacuum manufacturing processes and cannot easily control the shape, size, and density of metallic NPs [11, 22]. Therefore, other nano materials are employed as nano-floating gate in NFGOFETMs, for example, semiconducting or metal oxide NPs, however, they are not widely used in storage devices [11, 23, 24]. Thus, it is urgent to find more suitable nano-floating gate materials for high performance device with multilevel storage. Recently, antimony-doped tin oxide (ATO) NPs, as a transparent conductive oxide, have been extensively applied in the fields of electronics, photonics, photovoltaics, sensing, and other electronic fields because of their good conductivity, easy synthesis, excellent chemical stability, high mechanical strength and low cost [25, 26]. Moreover, ATO NPs material is a kind of NPs with small particle size and highly dispersible in water (green solvent), and more importantly, it can be deposited by solution-processing, which is benefit for realizing low-cost large-area organic electronics [27–29]. These properties of ATO NPs make them suitable candidate as a nano-floating gate layer in NFGOFETM devices. However, to the best of our knowledge, ATO NPs have not yet been used in NFGOFETM devices. Hence, it is extremely significant to open new doors for employing the ATO NPs in other electronic applications.

In addition, according to recent studies, it is found that light can be utilized as an individual elimination method to realize a photo-erasing process in OFET memories [30–35]. For example, Jang *et al* reported photo erasable memories based on OFETs by surface modified quantum-dot floating gates [35]. Liou *et al* demonstrated photoinduced-reset OFET memories based on a novel polymer electret [32]. Liao *et al* reported the transistor-type photoinduced-reset memories using a two-dimensional $Cs_2Pb(SCN)_2Br_2$/polymer as the floating gate [30]. These devices possess a 'photoinduced-reset' mechanism, which implements a photo-erasing process through photoinduced charge transfer between the organic semiconductor and floating gate layers. Compared to conventional electrically erasable devices, these 'photoinduced-reset' memories possess remarkable advantages regarding energy savings, convenient elimination of stored charges, and extended application as a photosensor. Therefore, it is significant to further introduce photoinduced-reset function into high performance NFGOFETMs.

In this work, a novel nonvolatile OFET memory device based on ATO NPs is demonstrated, in which 2, 7-dioctyl[1] benzothieno[3, 2-b][1]benzothiophene (C8-BTBT) is chosen as the organic semiconducting layer. The absorption of C8-BTBT is in the ultraviolet (UV) region, which indicates that UV light could be applied as an alternative to electrical operation [30–33]. Thus, the device possesses photoinduced-reset capacity, resulting in energy savings and convenient elimination of stored information [34, 35]. In addition, the resulting NFGOFETM devices exhibited outstanding memory properties, including tremendous memory window (~85 V), superhigh memory on/off ratio (~10^9), excellent data retention (over 10 years) and eminent multilevel storage ability. The overall performances of our devices are among the optimal performances in NFGOFETM devices based on OFETs as illustrated in table 1 [11, 31, 34–37]. This work demonstrates that ATO NPs with excellent comprehensive properties can be introduced as new charge trapping agent for memory devices and provide novel avenues for the manufacture of simple and low-cost data storage devices.

2. Experimental section

2.1. Materials

Polystyrene (PS, $Mw = 280\,000$, 99%) and C8-BTBT (99%) were purchased from Sigma Aldrich. ATO NPs and toluene were purchased from Aladdin. Highly doped n-type Si wafers with 300 nm thick SiO_2 were used as substrates. All solvents and regents were used without further purification.

2.2. Fabrication of the NFGOFETM

SiO_2/Si substrates were cleaned with deionized water, isopropyl alcohol, acetone and ethanol for 20 min each in an ultrasonic cleaner. The ATO NPs were dispersed in deionized water into 2.5, 5 and 7.5 mg ml^{-1}. After the substrates were treated with ultraviolet ozone for 15 min, the ATO NPs solution was spin-coated on the substrates at 3000 rpm for 60 s and was baked at 150 °C for 30 min on the hotplate to evaporate the water thoroughly. Then, the PS solution (2.5 mg ml^{-1}, toluene) was spin-coated onto the ATO NPs thin film with 3000 rpm for 60 s and they were baked at 80 °C for 60 min. The C8-BTBT film was fabricated on the PS film by thermal evaporation under vacuum (9.0×10^{-5} Pa). The thickness of PS and C8-BTBT are 6 and 74 nm, respectively. Finally, patterned gold source–drain electrodes were deposited by vacuum thermal evaporation through a shadow mask with channel lengths (L) and widths (W) of 90 and 4500 μm, respectively.

2.3. Characterization

The electrical measurements of NFGOFETM devices were conducted in ambient atmosphere using a Keysight B1500A semiconductor parametric analyzer. The UV–vis absorption spectra of ATO NPs and C8-BTBT were recorded on a PerkinElmer UV–vis lambda 365 spectrophotometer. The surfaces of ATO NPs films were characterized using a field emission scanning electron microscope (ZEISS Gemini SEM 300). The morphologies of C8-BTBT films were determined with atomic force microscopy (AFM, MFP-3D infinity). The light source was LED with the wavelength of 365 nm. The illumination intensity was measured by irradiatometers (THORLABS PM100D).

3. Results and discussion

The schematic diagram of the NFGOFETM device based on ATO NPs is illustrated in figure 1(a). Figure 1(b) displays the UV–vis absorption spectra of ATO NPs and C8-BTBT. It can be seen that the C8-BTBT possesses a distinct absorption peak at 361 nm and ATO NPs film has almost no absorption in the entire UV–vis absorption range, which suggests that ATO NPs film is a transparent material. Figures 1(c)–(e) show the AFM height images of C8-BTBT film on PS-ATO NPs films, in which the concentrations of ATO NPs solution are 2.5, 5 and 7.5 mg ml^{-1}, successively. It is found that the layered grains of C8-BTBT are clearly on these PS-ATO NPs films, indicating that good alignment of the molecules deposited on PS-ATO NPs films, which is very important to obtain high performance floating gate memory. As depicted in figures 2(a)–(d), the SEM images confirm the existence of ATO NPs with different densities. The SEM images also show that the densities and distribution of ATO NPs are in good agreement with their concentrations, as depicted in figures 2(a)–(c). It should be noted that the white dots with low density in figures 2(a)–(c) are the ATO NPs aggregates rather than ATO NPs. To more clearly understand the nanoscale structures of the ATO NPs aggregates, higher magnification SEM was further applied on a selected ATO NPs aggregate, as shown in figure 2(d). Interestingly, although the distribution of ATO NPs aggregates is not completely uniform, the ATO NPs in a single ATO NPs aggregate present relatively uniform distribution with the similar size of about tens of nanometers and the exact size distribution range of ATO NPs is shown in figure S1 (available online at stacks.iop.org/NANO/33/025201/mmedia) (corresponding to the SEM diagram in figure 2(d)). Furthermore, the distances between most ATO NPs in an aggregates range from several nanometers to tens of nanometers. These phenomena indicate that ATO NPs are suitable for the application in current transistor memories.

Bottom-gate top-contact C8-BTBT OFETs were fabricated with and without ATO NPs. The typical p-channel transistor behaviors are observed for all of the transfer curves and the drain voltage (V_D) is fixed at −40 V, as shown in figure 3 and figure S2. The OFET performance of the devices are summarized in table S1. We can find that the mobility of the device without ATO NPs is 3.8 $cm^2\,V^{-1}\,s^{-1}$, which is the highest among the four devices. When the ATO NPs floating gates are added to the devices, the mobilities decrease to different extent. The mobilities of the devices with 2.5, 5, 7.5 mg ml^{-1} ATO NPs are 3.5, 2.9 and 0.5 $cm^2\,V^{-1}\,s^{-1}$, respectively. Therefore, when the density and size of ATO NPs aggregates are small, the device still can maintain high mobility, such as the devices with 2.5 and 5 mg ml^{-1} ATO NPs. When the density and size of ATO NPs aggregates are too large, the mobility greatly reduced, such as the device with 7.5 mg ml^{-1} ATO NPs. Similarly, we can find that the relationship between the values of $I_{on/off}$ of the devices and size of the ATO NPs aggregates is the same. We further analyze the reasons for these effects on mobility. In our memory device, PS/C8-BTBT interface belongs to the organic semiconductor layer/dielectric interface of OFET. In OFET, the organic semiconductor layer/dielectric interface is an important interface that dominates carrier transport [38]. As the thickness of the tunneling layer PS is very thin, only 6 nm, and the size of the ATO NPs and its aggregates in the floating gate layer are much larger than 6 nm, resulting in uneven and rough surface. However, based on previous studies, flat and smooth surface morphology of the dielectric layer is very important to obtain high field effect mobility. Therefore, with the increase of the density and size of the ATO NPs aggregates, much rougher surfaces are introduced, resulting in the degradation of the mobility [11, 39–42].

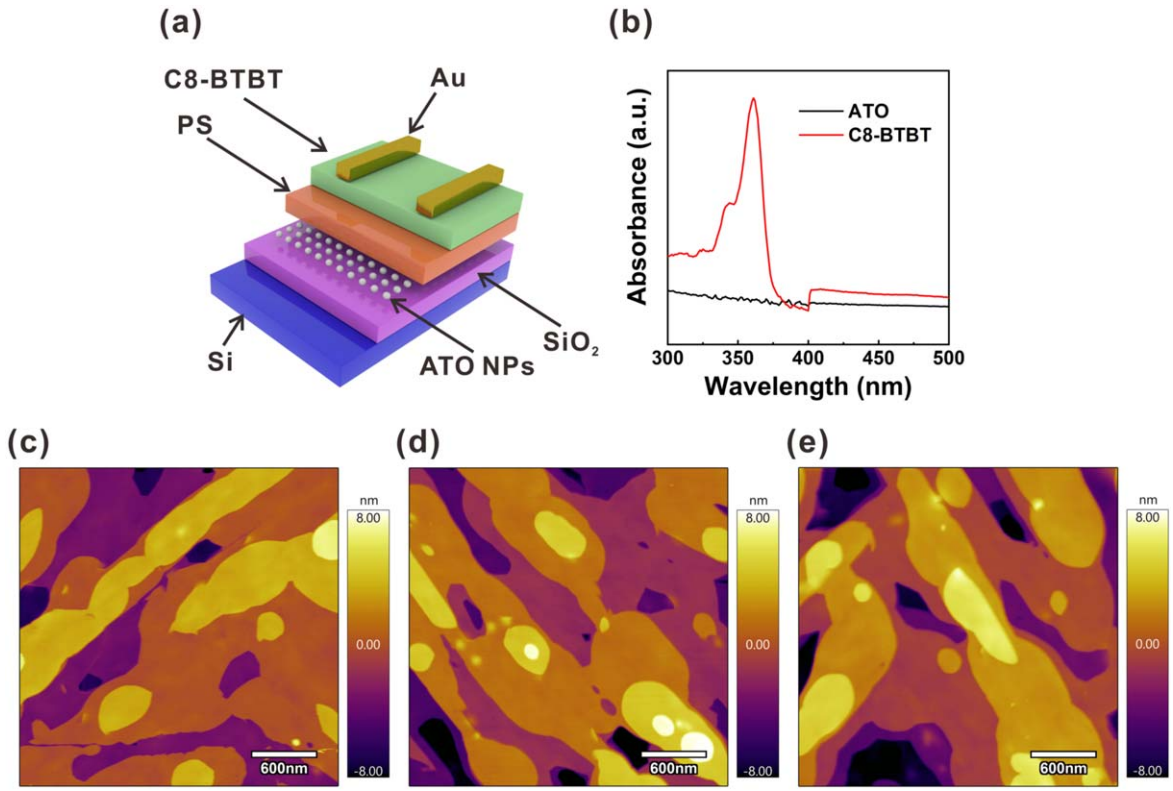

Figure 1. (a) Schematic illustration of the NFGOFETMs with ATO NPs floating gate. UV–vis absorption spectra of (b) ATO NPs and C8-BTBT film. (c)–(e) AFM images of C8-BTBT film on the PS-ATO NPs films (The concentration of ATO NPs solution is 2.5, 5 and 7.5 mg ml^{-1}, successively).

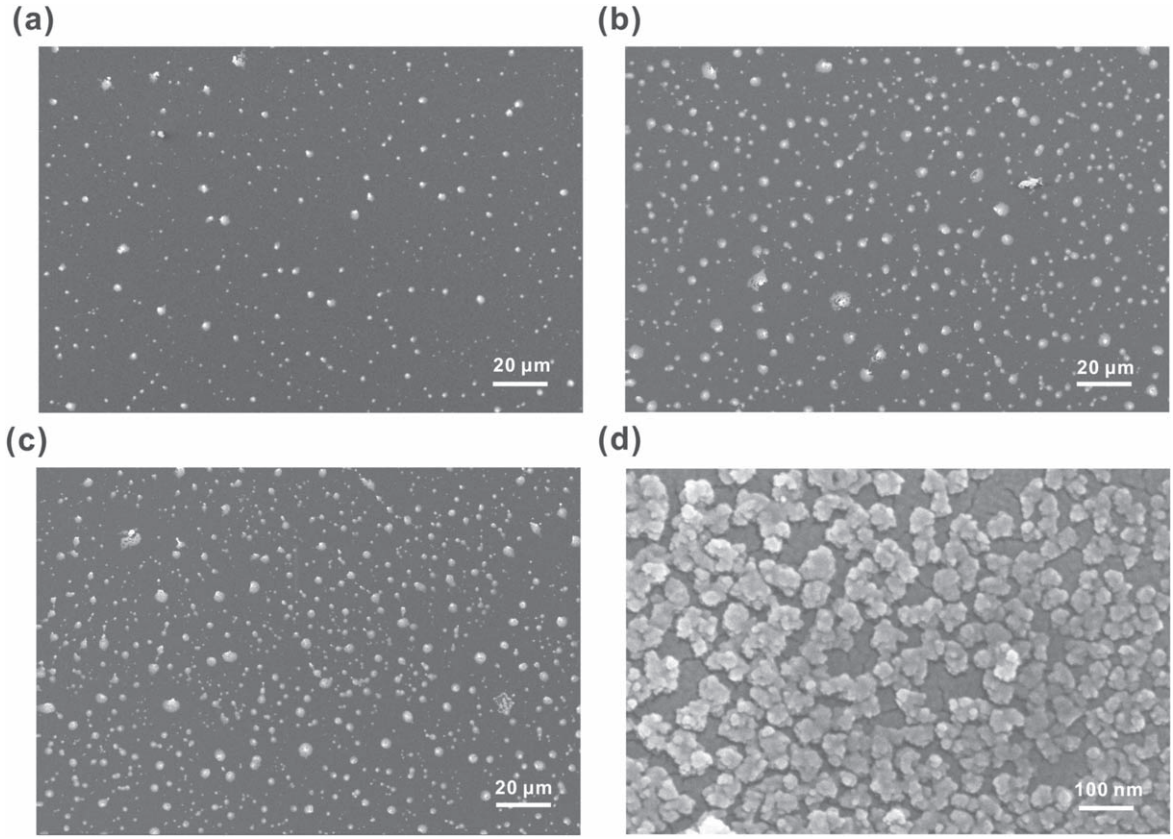

Figure 2. SEM images of ATO NPs with (a) 2.5 mg ml^{-1}, (b) 5 mg ml^{-1}, (c) 7.5 mg ml^{-1} on SiO_2/Si substrates and (d) higher magnification SEM image of 5 mg ml^{-1} ATO NPs on SiO_2/Si substrates.

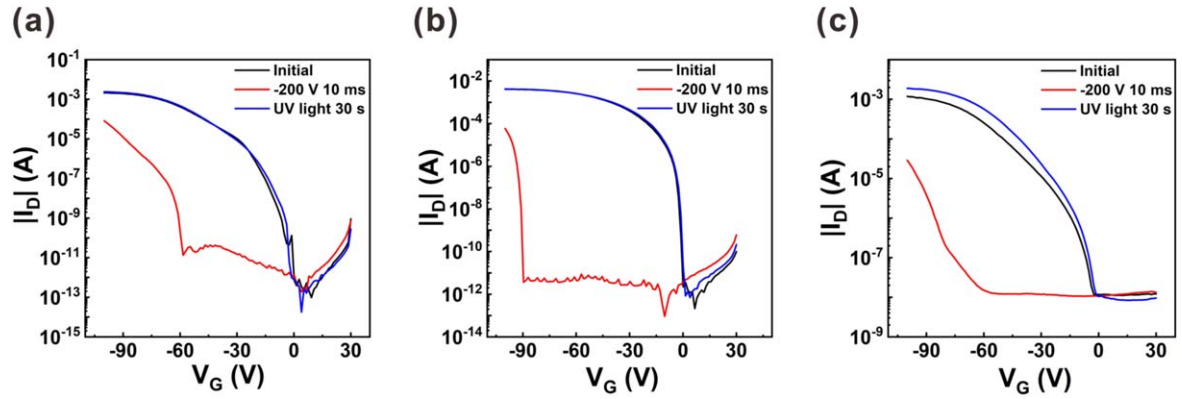

Figure 3. Transfer characteristics of the NFGOFETM devices with different ATO NPs concentrations ($V_D = -40$ V) (a) 2.5 mg ml^{-1}, (b) 5 mg ml^{-1} and (c) 7.5 mg ml^{-1}.

We further investigated the effect of the density of ATO NPs on the memory characteristics of devices. As a negative gate bias $V_G = -200$ V is exerted on the devices for only 10 ms, holes transfer from C8-BTBT and are trapped into the ATO NPs, which suppresses the formation of hole channel in C8-BTBT and leads to the negative shifts of transfer curves in figure 3. Interestingly, the transfer curves of the NFGOFETM devices can shift back to their initial states after exposing to UV light (365 nm) with an intensity of 3.5 mW cm^{-2} for 30 s, indicating that UV light could be used as the driving force to completely replace the electrical responses. The connection diagram of the device for electrical measurements in figure S3. The memory windows of the NFGOFETM based on 2.5, 5 and 7.5 mg ml^{-1} ATO NPs are 50.62, 84.77 and 68.33V, respectively. And their memory on/off ratios are 2.97 $\times$ 10^7, 1.10 $\times$ 10^9 and 3.85 $\times$ 10^4, respectively. The device based on ATO NPs with a concentration of 2.5 mg ml^{-1} obtains small memory window and memory on/off ratio, which may result from less charge trapping sites provided by less ATO NPs [43–45]. In another case, it is noteworthy that higher off current and suppressed memory window are observed in the device with a concentration of 7.5 mg ml^{-1}, compared to the device with 5 mg ml^{-1} ATO NPs. We speculate that this phenomenon may be caused by the following reason. As the density of ATO nanoparticles increases, the distance between ATO nanoparticles decreases and even connects, which eventually enhances the holes conduction between adjacent NPs and reduce the charge trapping efficiency [46]. Therefore, among these three concentrations, the NFGOFETM devices based on 5 mg ml^{-1} ATO NPs exhibit the best memory characteristics, including tremendous memory window (~85 V) and superhigh memory on/off ratio over 10^9, indicating its outstanding hole trapping capability. The trapped charge density (Δn) was roughly calculated according to the following equation:[47]

$$\Delta n = \frac{\Delta V_{th}}{e} C_i,$$

where e is the element charge, ΔV_{th} is the shift of threshold voltage and C_i is the capacitance of the gate dielectric. The trapped charge density is calculated to be about 6.0 $\times$ 10^{12} cm^{-2}. Moreover, in order to explore whether the size and density distribution of ATO NPs in our work can make the memory have uniform threshold voltage shifts, we tested ten devices at random positions on the same Si/SiO_2 substrate. Figure S4 shows threshold voltage shifts of the ten devices and the value of threshold voltage shifts are all about 85 $\pm$ 5 V. Thus, threshold voltage shifts for our memory devices based on ATO NPs are almost uniform. The distribution of memory windows in terms of volts is displayed in figure S5.

In order to quantify the contribution of ATO nanoparticle film versus SiO_2 dielectric towards threshold voltage shift, we perform control experiments by blank OFET memory without depositing ATO nanoparticle floating gate. Other than ATO nanoparticle film, the rest functional layers of the devices are the same. Figure S6 shows the electrical transfer characteristics of the device. The memory window of the blank device turned out to be notably narrower than the completed memory device. Under the application of programming voltage of $V_{G,pro} = -200$ V, the memory window of the completed OFET is ~85 V (figure 3(b)), being much larger than that from the blank device, ~10 V (figure S6). Obviously, the large memory window comes from ATO NPs floating gate.

These excellent memory characteristics make the device a suitable candidate for the realization of multilevel data storage with distinguishable memory states. Therefore, we further investigated the transfer characteristics of the device after applying varied programming gate voltages of $V_{G,Pro} = -100, -120, -140, -160, -180, -200$ V, $t = 10$ ms and UV light illumination for erasing process, at $V_D = -40$ V. The corresponding log plot of I_D and $\sqrt{I_D}$ versus $V_{G,Pro}$ are shown in figures 4(a) and (b), respectively. As the larger negative programming gate voltages are applied, the greater the shift of the transfer curves to the negative direction, which manifests that the trapping density of holes transferred from C8-BTBT into the ATO NPs can be controllable. To realize multilevel data storage, besides the aforementioned superhigh memory on/off ratio and tremendous memory window, long retention time and good durability are also required. Cycling tests by repetitively programming/erasing (P/E) procedures are illustrated in figures 4(c) and (d). Then, four distinct current states (different $V_{G,Pro}$ values of -120, -160, -200 V and photo-induced-reset behavior (365 nm, 3.5 mW cm^{-2}, 30 s)) of the

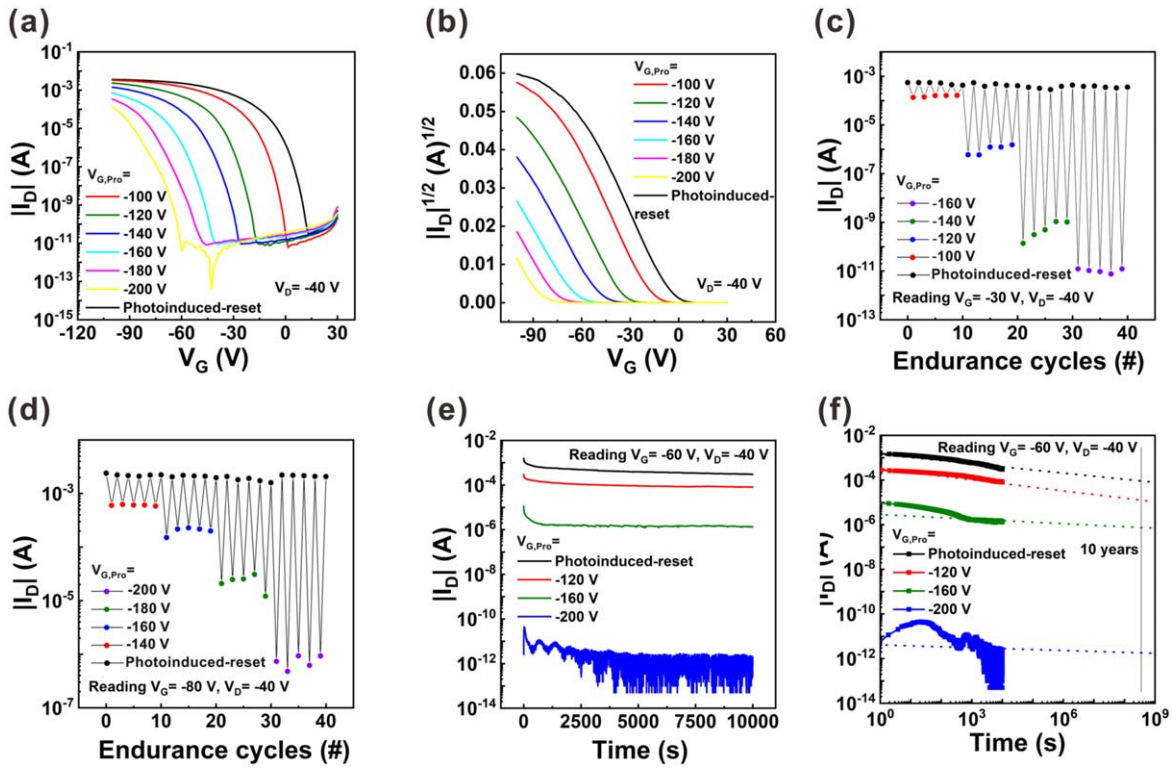

Figure 4. (a) $I-V$ characteristics and (b) $\sqrt{I}-V$ characteristics of the NFGOFETM devices $V_D = -40$ V. P/E switching cycles (c) at $V_G = -30$ V, $V_D = -40$ V and (d) at $V_G = -80$ V, $V_D = -40$ V. (e) Time dependent retention properties of 4 current levels (f) estimated retention time by extrapolation of each on- and off-state plot.

retention capabilities of the NFGOFETM are shown in figure 4(e). The retention time test indicated that the 4 current states are distinguishable and well sustained even after 10 000 s without obvious degradation. Importantly, the retention time estimated from the measured data would be more than 10 years, as shown in figure 4(f), which still shows its highly stable and distinguishable charge storage characteristics. In short, the memory devices possess good stability of data storage for practical applications.

In addition, we further decrease the operating voltages to explore the memory performance of the NFGOFETM devices. We measured the transfer characteristics of the device at $V_D = -10$ V, after applying $V_{G,Pro} = -80$, -100, -120, -140, -160, -180 or -200 V, $t = 10$ ms and UV light illumination (365 nm) for erasing process, as shown in figures S7(a), (b). The values of the memory window and memory current ratio were obtained with values of 11 V and 2.7×10^4, respectively, at the low operation voltages of $V_D = -10$ V and $V_{G,Pro} = -80$ V, and with the increase of programming voltages, the values of the memory window and memory current ratio increase successively. Cycling tests and the retention time test are illustrated in figures S7(c), (d), (e), which shows that the devices also have highly stable and distinguishable charge storage characteristics at lower $V_D = -10$ V.

The potential operation mechanism of the NFGOFETM was further investigated. Ultraviolet photoelectron spectroscopy (UPS) was used to determine the energy level of ATO NPs and C8-BTBT. As depicted in figure 5(a), the highest occupied molecular orbital (HOMO) energy level of C8-BTBT is estimated to be -5.34 eV according to the equation, ionization potentials (IP) $= h\nu - (E_{cutoff} - E_{H,onset})$. Combing with the calculated optical bandgap of C8-BTBT (3.34 eV) in figure 5(b), the lowest unoccupied molecular orbital (LUMO) energy level of C8-BTBT is estimated to be -2.00 eV. Au has high work function (5.1 eV) [48]. From the difference between the work function of Au electrodes and the HOMO energy level, it can be obtained that the low injection barrier of holes injected from Au into C8-BTBT is 0.24 eV, which allows the effective hole injection. Figure 5(c) shows the UPS spectra of the ATO NPs and the work function of ATO thin films is estimated to -4.77 eV. The HOMO and LUMO energy levels of C8-BTBT are -5.34 eV and -2.00 eV, respectively. And the thin PS tunneling layer (6 nm) is a wide band gap insulator material [37, 49]. The work function (-4.77 eV) of ATO NPs is slightly higher than HOMO (-5.34 eV) of C8-BTBT. The C8-BTBT layer, PS layer, and ATO NPs layer are independent layers. Figure 5(d) shows the energy band diagram of PS, C8-BTBT and ATO NPs in the flat band state without $V_{G,pro}$. During the programming process (figures 5(e), S8(a)), as a negative $V_{G,pro}$ is applied to the NFGOFETM devices in darkness, the energy bands of C8-BTBT and PS are bent and the corresponding interfacial barriers are overcome, thus the holes can be injected from the HOMO of C8-BTBT into the deep-level states of the ATO NPs through a thin PS tunneling layer. PS, the wide band gap insulating polymer with ultra-deep HOMO level, prevented vertical leakage of the trapped

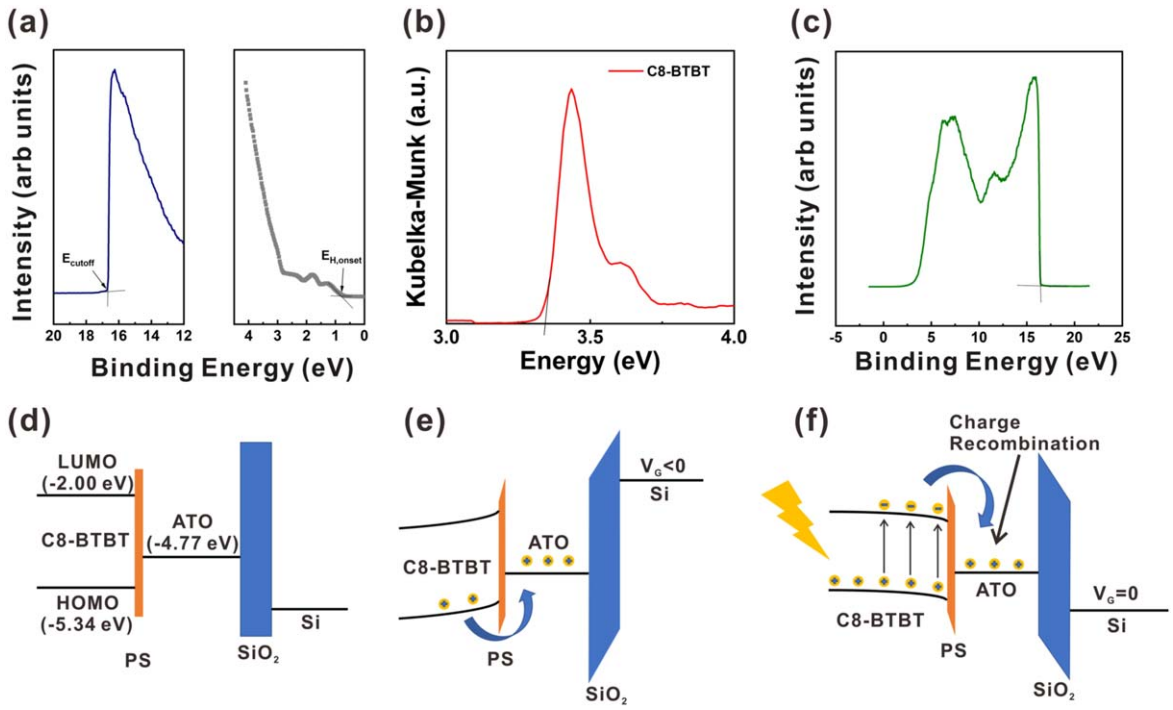

Figure 5. (a) Ultraviolet photoelectron spectroscopy (UPS) spectra of C8-BTBT, (b) optical absorption spectra of C8-BTBT, (c) UPS spectra of ATO NPs. Energy band diagram of (d) C8-BTBT and ATO NPs at $V_G = 0$, and (e) during program operation ($V_G < 0$), and (f) during erase operation (under light) for the charge trapping/releasing mechanism.

holes between ATO NPs and the C8-BTBT [50]. According to the previous studies [51, 52], for floating gate organic memory, the charge tunneling could be divided into direct tunneling and Fowler Nordheim tunneling (FN tunneling). In the direct tunneling mechanism, the thickness of a tunneling layer is thin (several nanometers) and the programming voltages are also relatively low. For the FN tunneling mechanism, the thickness of the tunneling layer is thick, thus it is difficult to realize efficient direct tunneling and the programming voltages are high. In our work, the PS solution (2.5 mg ml^{-1}, toluene) was spin-coated (3000 rpm, 60 s) to form the tunneling layer. The tunneling layer thicknesses is only 6 nm, which can cause carriers direct tunneling. In addition, as shown in figure 5(e), the energy band of PS layer is bent under the high programming operation voltage, leading to the holes in the HOMO energy level of C8-BTBT transfer to ATO NPs mainly through FN tunneling. Therefore, both direct tunneling and FN tunneling mechanisms exist in our memory devices. Consequently, the trapped holes in ATO NPs floating gate would form E_{in} between C8-BTBT and ATO floating gate (figure S8(a)) and the transfer curve of the NFGOFETM shifted to the negative direction [7, 53, 54].

For the erasing operation in figures 5(f), S8(b), light-only bias is applied for holes to be detrapped. As shown in figure 1(b), C8-BTBT possesses a distinct absorption peak at 361 nm, while the ATO NPs has no absorption. In this work, the photon energy (3.40 eV) of the incident UV light is larger the band gap (3.34 eV) of C8-BTBT and there is an E_{in} to prompt carrier separation and transfer. Moreover, the thickness of the PS tunneling layer is very thin (6 nm). According to previous important studies, these situations mentioned above significantly improve direct tunneling transfer of the photogenerated carriers at zero bias [52]. Therefore, it can be concluded that the photoinduced-reset mechanism of this work is that when the NFGOFETM is illuminated by UV light (365 nm), excitons generate initially in C8-BTBT and move to the C8-BTBT/PS interface. Then, the excitons are quickly divided into photo-generated holes and electrons and driven by the E_{in}, photo-generated electrons enter the ATO NPs floating gate layer by direct tunneling though PS layer to recombine with holes trapped in deep-level states of ATO NPs [34, 35, 53]. And the photo-generated holes drift toward C8-BTBT to increase the concentration of holes in the conductive channel. As a result, the trapped holes are finally erased in the ATO NPs and the concentration of holes in the conductive channel of C8-BTBT return to the original state. Thus, the transfer curves of the NFGOFETM shifted back to its initial state.

4. Conclusions

High-performance NFGOFETM devices are fabricated using C8-BTBT and ATO NPs as the organic semiconductor and floating gate, respectively, in which ATO NPs have been used as floating gate material for the first time. The NFGOFETM exhibits outstanding overall performances, including tremendous memory window (~85 V), superhigh memory on/off ratio (~10^9), excellent data retention (over 10 years) and eminent multilevel storage ability, which are among the optimal performances in NFGOFETM devices based on OFETs. Furthermore, the 'photoinduced-reset' behavior could

be obtained in NFGOFETMs under UV light. This work demonstrates that ATO NPs can be introduced as new charge trapping agents for memory devices and provide novel avenues for the manufacture of simple and low-cost fabrication of data storage devices with multilevel storage and photo-induced-reset behaviors.

Acknowledgments

The authors would like to acknowledge the financial support from National Natural Science Foundation of China (No. 22005270), Zhejiang Provincial Natural Science Foundation of China (No. LQ21E030003), the Education Department Program of Zhejiang Province, China (No. Y201943039), the National Key R&D Program of China (2018YFB1500102), Zhejiang Provincial Key Laboratory (No. 2013E10022).

Data availability statement

All data that support the findings of this study are included within the article (and any supplementary files).

Declaration of interests

The authors declare that they have no known competing financial interests or personal relationships that could have appeared to influence the work reported in this paper.

ORCID iDs

Keli Shi https://orcid.org/0000-0002-1440-4132
Shihua Huang https://orcid.org/0000-0003-1727-2232

References

[1] Unni K N N, Bettignies R, Dabos-Seignon S and Nunzi J-M 2004 *Appl. Phys. Lett.* **85** 1823
[2] Qian Y, Zhang X, Xie L, Qi D, Chandran B K, Chen X and Huang W 2016 *Adv. Mater.* **28** 9243
[3] Shi W, Guo Y and Liu Y 2020 *Adv. Mater.* **32** 1901493
[4] Wei Q, Lin Y, Anderson E R, Briseno A L, Gido S P and Watkins J J 2012 *ACS Nano* **6** 1188
[5] Kim Y-J, Kang M, Lee M-H, Kang J-S and Kim D-Y 2020 *Adv. Electron. Mater.* **6** 2000189
[6] Shih C-C, Lee W-Y and Chen W-C 2016 *Mater. Horiz.* **3** 294
[7] Che Y, Zhang Y, Cao X, Song X, Cao M, Dai H, Yang J, Zhang G and Yao J 2016 *Appl. Phys. Lett.* **109** 013106
[8] Yan C, Wen J, Lin P and Sun Z 2019 *Small* **15** 1804156
[9] Zhou L, Mao J, Ren Y, Han S-T, Roy V A L and Zhou Y 2018 *Small* **14** 1703126
[10] Hu D, Wang X, Chen H and Guo T 2017 *Adv. Funct. Mater.* **27** 1703541
[11] Jung J H, Kim S, Kim H, Park J and Oh J H 2015 *Small* **11** 4976
[12] Cai J, Fang B, Wang C and Zeng Z 2017 *Appl. Phys. Lett.* **111** 182410
[13] Lim S H, Lee J B, Kim G M and Ahn W H 2020 *IEEE Access* **8** 162491
[14] Wu X, Lan S, Hu D, Chen Q, Li E, Yan Y, Chen H and Guo T 2019 *J. Mater. Chem.* C **7** 9229
[15] Yang H, Yan Y, Wu X, Liu Y, Chen Q, Zhang G, Chen S, Chen H and Guo T 2020 *J. Mater. Chem.* C **8** 2861
[16] Guo Y, Di C-A, Ye S, Sun X, Zheng J, Wen Y, Wu W, Yu G and Liu Y 2009 *Adv. Mater.* **21** 1954
[17] Lee D, Hwang E, Lee Y, Choi Y, Kim J S, Lee S and Cho J H 2016 *Adv. Mater.* **28** 9196
[18] Tran C M, Sakai H, Kawashima Y, Ohkubo K, Fukuzumi S and Murata H 2017 *Org. Electron.* **45** 234
[19] Shen J-X, Shang D-S, Chai Y-S, Wang S-G, Shen B-G and Sun Y 2018 *Adv. Mater.* **30** 1706717
[20] Minnekhanov A A, Emelyanov A V, Lapkin D A, Nikiruy K E, Shvetsov B S, Nesmelov A A, Rylkov V V, Demin V A and Erokhin V V 2019 *Sci. Rep.* **9** 10800
[21] Kang M, Baeg K-J, Khim D, Noh Y-Y and Kim D-Y 2013 *Adv. Funct. Mater.* **23** 3503
[22] Zhu Z, Guo Y and Liu Y 2020 *Mater. Chem. Front.* **4** 2845
[23] Verrelli E, Tsoukalas D, Normand P, Kean A and Boukos N 2013 *Appl. Phys. Lett.* **102** 022909
[24] Maikap S, Wang T, Tzeng P, Lin C, Lee L, Yang J and Tsai M 2007 *Appl. Phys. Lett.* **90** 253108
[25] Zheng M and Wang B 2009 *Trans. Nonferr. Met. Soc.* **19** 404
[26] Jain G and Kumar R 2004 *Opt. Mater.* **26** 27
[27] Luo S-X, Song Z and Li J-L 2013 *J. Funct. Mater.* **11** 1603
[28] Sun H, Liu B, Liu X and Yin Z 2017 *J. Mater. Res.* **32** 2414
[29] Jung D-W and Park D-W 2009 *Appl. Surf. Sci.* **255** 5409
[30] Liao M-Y, Chiang Y-C, Chen C-H, Chen W-C and Chueh C-C 2020 *ACS Appl. Mater. Inter.* **12** 36398
[31] Li Q, Li T, Zhang Y, Chen Z, Li Y, Jin L, Zhao H, Li J and Yao J 2020 *J. Phys. Chem.* C **124** 23343
[32] Chen C H, Wang Y, Tatsumi H, Michinobu T, Chang S W, Chiu Y C and Liou G S 2019 *Adv. Funct. Mater.* **29** 1902991
[33] Yi M, Xie M, Shao Y, Li W, Ling H, Xie L, Yang T, Fan Q, Zhu J and Huang W 2015 *J. Mater. Chem.* C **3** 5220
[34] Jeong Y J, Yun D-J, Kim S H, Jang J and Park C E 2017 *ACS Appl. Mater. Inter.* **9** 11759
[35] Jeong Y J, Yun D-J, Noh S H, Park C E and Jang J 2018 *ACS Nano* **12** 7701
[36] Shih C-C, Chiu Y-C, Lee W-Y, Chen J-Y and Chen, W-C 2015 *Adv. Funct. Mater.* **25** 1511
[37] Chen J-Y, Chiu Y-C, Li Y-T, Chueh C-C and Chen W-C 2017 *Adv. Mater.* **29** 1702217
[38] Di C-A, Liu Y, Yu G and Zhu D 2009 *Acc. Chem. Res.* **42** 1573
[39] Han S-T, Zhou Y, Wang C, He L, Zhang W and Roy V A L 2013 *Adv. Mater.* **25** 872
[40] Weis M, Manaka T and Iwamoto M 2010 *IEEJ Trans Elec Electron Eng* **5** 391
[41] Kang S J, Lee G-H, Yu Y-J, Zhao Y, Kim B, Watanabe K, Taniguchi T, Hone J, Kim P and Nuckolls C 2014 *Adv. Funct. Mater.* **24** 5157
[42] Shahbazia M, Baharia A and Ghasemib S 2016 *Synth. Met.* **221** 332
[43] Kang M, Kim Y-A, Yun J-M, Khim D, Kim J, Noh Y-Y, Baeg K-J and Kim D-Y 2014 *Nanoscale* **6** 12315
[44] Han S-T, Zhou Y, Chen B, Zhou L, Yan Y, Zhang H and Roy V A L 2015 *Nanoscale* **7** 17496
[45] Chang H-C, Liu C-L and Chen W-C 2013 *ACS Appl. Mater. Inter.* **5** 13180
[46] Han S-T, Zhou Y, Xu Z-X, Roy V A L and Hung T F 2011 *J. Mater. Chem.* **21** 14575
[47] Baeg K-J, Noh Y-Y, Sirringhaus H and Kim D-Y 2010 *Adv. Funct. Mater.* **20** 224
[48] Kan J, Chen Y, Qi D, Liu Y and Jiang J 2012 *Adv. Mater.* **24** 1755

[49] Aimi J, Lo C-T, Wu H-C, Huang C-F, Nakanishi T, Takeuchi M and Chen W-C 2016 *Adv. Electron. Mater.* **2** 1500300
[50] Xu T, Guo S, Qi W, Li S, Xu M, Xie W and Wanga W 2020 *Appl. Phys. Lett.* **116** 023301
[51] She X-J, Liu C-H, Sun Q-J, Gao X and Wang S-D 2012 *Org. Electron.* **13** 1908
[52] Guo X, Zhang W, Yin J, Xu Y, Bai Y and Yang J 2021 *Org. Electron.* **93** 106149
[53] Jin R, Wang J, Shi K, Qiu B, Ma L, Huang S and Li Z 2020 *RSC Adv.* **10** 43225
[54] Ling H, Lin J, Yi M, Liu B, Li W, Li Z, Xie L, Bao Y, Guo F and Huang W 2016 *ACS Appl. Mater. Inter.* **8** 18969